Original Research Article

Liquid jet breakup unsteadiness in a coaxial air-blast atomizer

Abhijeet Kumar and Srikrishna Sahu ⬛

Abstract

The aim of this paper is to experimentally characterize the liquid jet breakup unsteadiness in a coaxial air-blast atomizer. The current research focuses on the measurement of the fluctuations of the jet breakup length and the flapping instability of the liquid jet, which contribute to the downstream fluctuations of the spray characteristics. The optical connectivity technique was used to measure the instantaneous breakup length of the water jet. Also, time resolved shadowgraph images of the primary jet breakup process were captured by high-speed imaging to characterize the jet instabilities at different axial locations from the atomizer exit. Experiments were performed for a wide range of air-to-liquid momentum flux ratio (M) and aerodynamic Weber number (We_g) corresponding to membrane- and/or fiber breakup mode of the jet disintegration process. The mean jet breakup length was found to vary inversely with M through a power law relation in agreement with the literature, while the breakup length fluctuations were found to first decrease and then increase with M. In order to capture the unsteady dynamics of the jet breakup process, the proper orthogonal decomposition analysis of the optical connectivity images was performed. The jet flapping and the fluctuations of the jet breakup length were identified as the second and the third spatial proper orthogonal decomposition modes, respectively, for all operating conditions of the atomizer. The amplitude and the frequency of the instabilities were measured by temporal tracking of the liquid–air interface on the shadowgraph images. The disturbance close to the injector exit corresponds to the Kelvin–Helmholtz instability, while close to the jet breakup point the jet exhibits the flapping instability, which is characterized by lateral oscillation of the jet about the atomizer axis. The influence of the liquid jet Reynolds number and momentum flux ratio on the KH and the flapping instabilities are examined.

Keywords

Optical connectivity, atomization, breakup length, flapping, proper orthogonal decomposition

1. Introduction

Air-blast atomization of liquid fuel jets is a crucial stage in the overall combustion process in various aero-propulsion systems. The coaxial configuration for air and fuel flow passages in the atomizers is relevant especially to liquid propelled rocket engines and also important for fundamental understanding of the jet breakup. The quality of atomization as a consequence of the liquid jet breakup close to the atomizer exit and the downstream droplet-air mixing is intimately related to the flame stability, overall performance and pollutant emission. The detailed understanding on the jet breakup process is important for control on the droplet size and the spatio-temporal distribution of the liquid mass near the reaction zone downstream of the atomizer exit. It is well known that typically the atomization of liquid jets occurs in two stages: the primary breakup of the liquid jet near the atomizer exit and the subsequent secondary breakup of the arbitrary shaped liquid ligaments as well as the large droplets generated from the primary breakup further downstream.[1] In the primary breakup region, the shear force at the liquid-gas interface is responsible for the disintegration of the

Department of Mechanical Engineering, Thermodynamics and Combustion Engine Lab, Indian Institute of Technology Madras, Chennai, India

Corresponding author:
Srikrishna Sahu, Department of Mechanical Engineering, Indian Institute of Technology Madras, Chennai 600036, India.
Email: ssahu@iitm.ac.in

liquid jet.[2–6] The extent of the primary atomization region is usually characterized by the jet breakup length, which is the length of the continuous liquid core corresponding to complete disintegration of the jet into droplets and ligaments. The liquid jet breakup length is typically few liquid jet diameters and in general, it depends on the liquid–gas relative velocity, the nozzle geometry and the physical properties of the two fluids[4,7,8] However, the primary breakup region can be additionally characterized by the unbroken length or liquid intact length referring to the axial location where breakup begins.[9] The primary breakup length is very important for the performance of the fuel injectors and also for the development of computational models of the atomization process for numerical simulation of sprays as it defines the beginning of the fully developed multiphase flow region. In past, several studies have reported measurement of liquid jet breakup length in air-blast atomizer.[1,4,8,10–12] Most of these studies are based on the shadowgraphic visualization of the jet. However, the presence of a dense cloud of droplets and ligaments around the liquid core often prevents accurate probing of the primary breakup region.[13] In addition, the previous studies reported the mean jet breakup length based on identification of the breakup point either through visual inspection or image processing of an ensemble of images. However, the liquid jet disintegration process being highly unsteady, the instantaneous jet breakup length may vary substantially with time. According to Chigier and Farago[14] and Chigier and Reitz,[15] the jet atomization is often a pulsating process leading to a periodical temporal change in the spray characteristics (such as liquid volume flux and droplet number density) downstream of the atomizer even when the inlet liquid and atomizing gas flows are steady, oscillation-free and vibration-free. The unsteady flow of the liquid fuel mass into the combustion chamber can be of significance to practical issues such as the combustion instability. Hence, in addition to the mean breakup length, characterization of the jet breakup length fluctuations is also important since it indicates downstream unsteadiness within the spray. While only few studies have reported such measurements in the past (for instance, Charalampous et al.[16]), a comprehensive study on the fluctuations of jet breakup length for a wide range of operating conditions of the atomizer is still lacking.

The disintegration of liquid jets in air-blast atomizers is a complex process. Depending on the operating flow conditions of the atomizer, the liquid jet is subjected to various instabilities including capillary, helical, Kelvin–Helmholtz (KH) instability, etc. and different mechanisms of breakup of the liquid core and ligaments have been identified in the earlier works. Such mechanisms are linked to the formation of disturbance waves on the liquid–air interface, which develop downstream of the injector and lead to the breakup of the liquid jet into ligaments and/or droplets after a critical waveform is reached.[1,4,14,17,18] Eroglu and Chigier[19] showed that the wave frequency near the nozzle exit increases with increasing the gas velocity. Villermaux et al.[20] identified the existence of low-frequency oscillations in addition to the KH frequency for velocity ratio of the annular fluid to the inner fluid more than six in their experiments. The studies on liquid sheets are also very relevant to understand the mechanisms of the instabilities. Villermaux and Clanet[21] showed that the sinuous unstable mode dominates over the dilatational mode of breakup of a liquid sheet. They also mentioned that the shear instability gave flag like motion to the liquid, thereby triggering Rayleigh–Taylor (RT) instability at the rim of sheet. Varga et al.[22] identified that close to the nozzle exit, due to amplification of the primary instability, the lateral segments of a liquid jet experience large acceleration in a direction perpendicular to their surfaces, making them susceptible to the RT instability. This mechanism is responsible for complete disintegration of the liquid jet into a fine spray within the potential cone of the large-diameter gas jet. Duke et al.[23] suggested two distinct physical sources of instability in liquid sheets, first being the well-known free shear instability, which is quasi-sinusoidal and nonlinear and the second being the nonlinear rupturing instability, which is modulated by the former. As far as primary breakup of liquid jets/sheets are concerned, there is no general consensus on the importance of RT in comparison to KH instability. Several earlier research works (for instance, Lasheras and Hopfinger[9]; Varga et al.[22]; Marmottant and Villermaux[24]) suggest that the KH instability is mostly responsible for primary atomization. As mentioned earlier, the finite amplitude of waves on the jet surface as well as jet flapping may trigger the RT instability leading to the generation of droplets and ligaments. However, the possibility of combined action of both instabilities has been discussed by Vadivukkarasan and Panchagnula[25]who developed a three-dimensional temporal stability model for the growth of the instability and identified short wavelength helical mode when both KH and RT mechanisms are active on the cylindrical liquid jet. Recently, Matas and Cartellier[26] recognized the flapping instability as a mechanism leading to oscillation of the tail of the liquid jet near the breakup point. This large-scale instability leads to generation of large liquid lumps near the breakup region. Odier et al.[27] did numerical study of a flapping liquid sheet and found that a vortical detachment of the high-speed air stream behind the interfacial wave modifies the pressure field around

the sheet which results in the flapping of the liquid sheet.

In spite of significant efforts in the past, the physics of the jet breakup process is not yet well known, and thorough understanding on the mechanisms of the jet breakup process is essential. Especially, though it is well known that the breakup of the liquid jet is a highly unsteady process, it's consequence on the spatio-temporal distribution of drop size, velocity, number density and liquid mass flux downstream of the atomizer is not yet well understood. However, for this purpose, detailed characterization of the jet breakup unsteadiness is essential. In the present paper, the focus is on the above, in particular, characterization of the jet breakup length fluctuations and flapping instability of the jet. Although the experimental correlations for the mean jet breakup length are available from the earlier works, any quantitative discussion on the fluctuation of the jet breakup length is not available. Similarly, there is no general consensus on the injector operating conditions susceptible to intense jet flapping. Thus, we have selected an atomizer for which a good account on the average jet breakup characteristics and some of the mechanisms of jet instabilities are available in the literature such that these can provide a reference compared with our new findings. In order to eliminate the influence of liquid evaporation, heat exchange and chemical reactions on the breakup process, the experiments were conducted under atmospheric conditions with water and air as the working fluid. The instantaneous jet breakup length was measured by the so called optical connectivity (OC) technique, which is advantageous in comparison to the conventional shadowgraph visualization since the liquid core region can be imaged specifically excluding the surrounding ligaments and droplets such that the jet breakup length can be measured with better accuracy. The mean as well as the fluctuations of the jet breakup length were measured over a wide range of the air-to-liquid momentum flux ratios. The proper orthogonal decomposition (POD) analysis of the OC images was carried out to understand the dynamics of different modes of the jet breakup process. The high-speed shadowgraph images were also captured to track the time dependent liquid–air interface at different axial locations downstream of the nozzle exit in order to characterize the dominant instability at those locations.

The paper is organized as follows. Section 2 includes the description of the experimental arrangement and the optical techniques used in the present study also give a brief overview on the image processing and the POD analysis. Section 3 presents the results on the measurement of liquid core region by the OC technique. The characterization of the jet instabilities by the high-speed shadow imaging appears in the same section. A summary of the work and the conclusions can be found in Section 4.

2. Experimental method

2.1. Air-blast Atomizer

A coaxial air-blast atomizer is considered (Figure 1) which incorporates a central metallic tube to allow the flow of the liquid to be atomized, while the atomizing air flows in a surrounding concentric annular passage. The air and the liquid jets interact only beyond the exit of the atomizer. The basic design of the atomizer is similar to Hardalupas and Whitelaw[28] and Engelbert et al.[5] The inner diameter of the central tube is 3 mm, whereas its outer diameter is 6 mm, respectively. A liquid jet of diameter, D_l, equals to 3 mm is issued at the atomizer exit. Around the central tube, the annular region (outer diameter, $D_o = 15$ mm, inner diameter, $D_i = 6$ mm; annular gap is 4.5 mm) provides air at much higher velocity than that of the liquid jet. The area contraction ratio for liquid is 28.4, and that for air passage is 17.1, respectively. An annular holder with straight vanes is used to support the central tube carrying the liquid. The atomizer was operated under atmospheric pressure and temperature conditions, and water and air were used as the working fluids.

2.2. Operating conditions of the atomizer

The non-dimensional numbers describing the atomizer operating flow conditions are the liquid flow Reynolds number (Re_l), aerodynamic Weber number (We_g) and
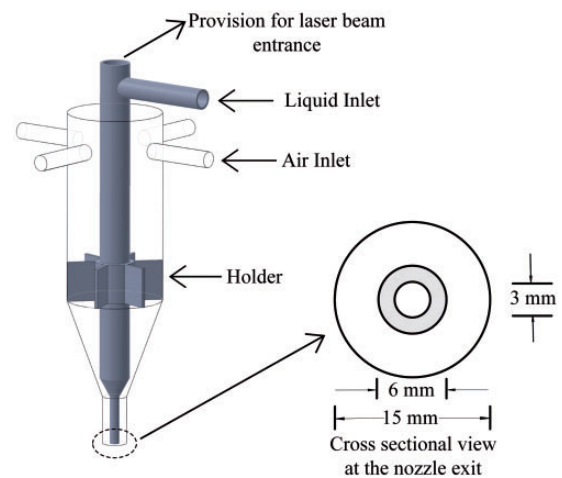

Figure 1. Schematic of the coaxial air-blast atomizer. The cross-sectional view at the nozzle exit is also shown.

air-to-liquid momentum flux ratio (*M*), which are expressed below

$$Re_l = \frac{U_l D_l}{\nu_l} \qquad (1)$$

$$We_g = \frac{\rho_g (U_g - U_l)^2 D_l}{\sigma} \qquad (2)$$

$$M = \frac{\rho_g U_g^2}{\rho_l U_l^2} \qquad (3)$$

where *U* represents the average fluid velocity at the atomizer exit, and ρ, ν and σ are the density, kinematic viscosity and surface tension of the fluids respectively. The subscript '*g*' and '*l*' under any quantity denote air and liquid, respectively. The volume flow rates of air and liquid were measured with respective rotameters. The average liquid and gas velocity (U_l and U_g) at the nozzle exit were calculated by dividing the volume flow rate by the cross-sectional area of their respective flow passages.

The atomizer is operated under 12 different flow conditions as outlined in Table 1. The relevant non-dimensional numbers for each flow condition are also shown in Table 1. The experiments are performed for a wide range of Weber number, We_g (80–300) and momentum flux ratio, *M* (1–8). The Re_l of the liquid jet is 3000–5000.

2.3. Optical arrangement and image processing

In the present experiments, the liquid core region during the primary breakup of the liquid jet was characterized by the application of the OC technique, while

Table 1. Operating flow conditions for the coaxial air-blast atomizer and the corresponding non-dimensional numbers.

Flow conditions	U_l (m/s)	U_g (m/s)	Re_l	We_g	M
1	0.9	42.1	3178	83.5	2.4
2	1.2	42.1	3972	82.6	1.5
3	1.4	42.1	4767	81.6	1.1
4	0.9	56.1	3178	150.2	4.2
5	1.2	56.1	3972	148.9	2.7
6	1.4	56.1	4767	147.6	1.9
7	0.9	70.2	3178	236.3	6.6
8	1.2	70.2	3972	234.7	4.7
9	1.4	70.2	4767	233.1	2.9
10	0.9	78.6	3178	297.2	8.3
11	1.2	78.6	3972	295.4	5.3
12	1.4	78.6	4767	293.6	3.7

the high-speed shadowgraph technique was used for the time resolved visualization of the jet breakup process.

The principle of the OC technique is based on imaging the laser-induced fluorescence (LIF) emitted from a stream of liquid doped with a suitable dye.[13] The technique takes advantage of the higher refractive index of the liquid in comparison to the surrounding air such that when the incident angle of the laser beam is greater than the critical angle for the total internal reflection, the laser beam is internally reflected in the liquid stream completely and propagates downstream for a long distance while being contained within the stream. Beyond the point of liquid discontinuity due to the jet breakup, the laser beam is diffused and its intensity is significantly reduced. This way, specifically the primary breakup region can be imaged by using a suitable optical filter specified by the wavelength of the emitted fluorescent light. A comparison of the liquid jet breakup length measurement by the OC technique with other approaches such as shadowgraphy and electrical connectivity techniques can be found in Charalampous et al.[29] Charalampous et al.[16] reported the application of the OC technique for measurement of the three-dimensional location of the liquid core of the continuous liquid jet by simultaneously imaging from the two different directions. Heilig et al.[30] applied the OC technique for the jet intact core length measurement in a multi-hole diesel injector. As the laser light was guided through an optical fiber into the injector to internally illuminate the jet(s), some modification of the injector was essential.

A schematic of the optical setup for the OC technique is shown in Figure 2. A pulsed Nd:Yag laser (Quantel, EverGreen:145 mJ/pulse at 532 nm; 5 mm beam diameter) was used to internally illuminate the liquid jet. The horizontal laser beam was diverted in perpendicular downward direction using a mirror. The atomizer has a provision to allow the laser beam from the top (see Figure 1) to illuminate the water in the central tube. Unlike Charalampous et al.,[13] no laser guide tube was used so that the internal flow modification within the atomizer is avoided. The water was tagged with the Rhodamine 6 G dye such that when the liquid jet is illuminated with the 532 nm green laser beam, the dye fluoresces. The fluorescent light is red-shifted (with peak at 555 nm), which was imaged by a CCD camera (PCO Pixelfly: 14 bit, 1040×1392 pixels^2). A long pass filter is used to suppress the scattered light from the liquid jet. The images were captured at the resolution of 45 μm/pixel. The OC technique is advantageous in comparison to the conventional shadowgraphy technique for primary breakup length measurement since the continuous liquid jet can be visualized without significant interference from the surrounding droplets or ligaments. Since
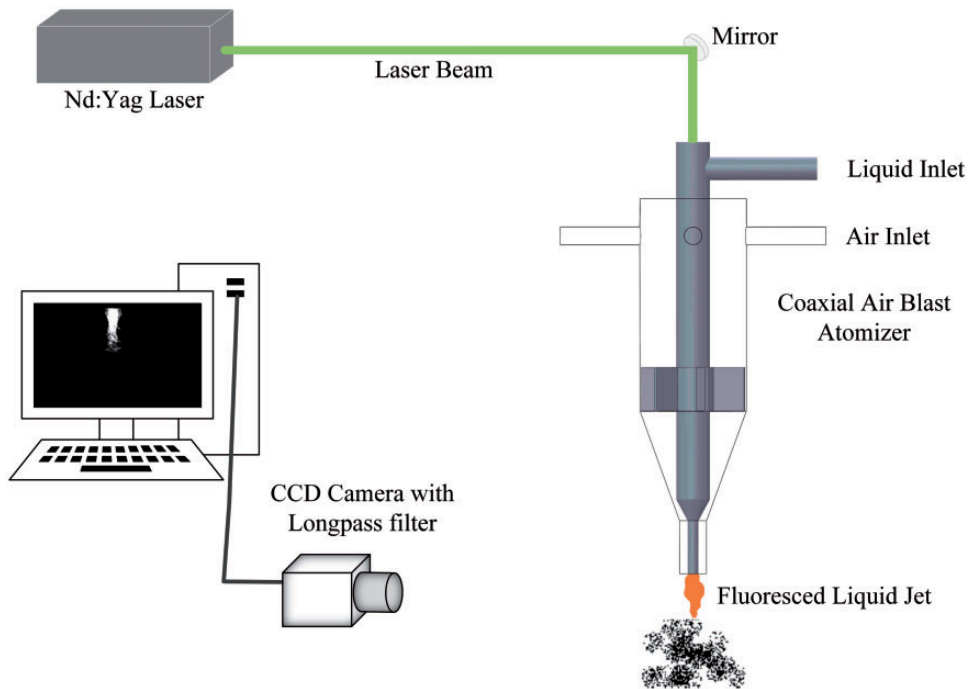
Figure 2. Schematic of the optical arrangement for application of the optical connectivity technique.
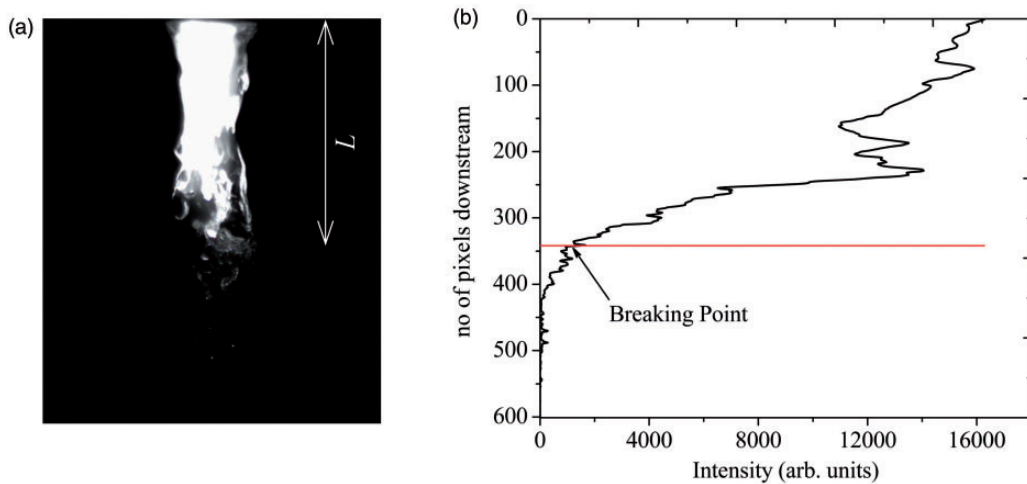

Figure 3. (a) A typical instantaneous OC image and (b) average intensity variation downstream from nozzle exit for the same image. The location of the breakup point and the liquid jet breakup length are also shown.

the detached liquid masses in the vicinity of the liquid core often obstruct the observation of the breakup point in normal shadowgraphy visualization, it may lead to significant error in the measurement of breakup length as demonstrated by Charalampous et al.[29] However, under rigorous atomizing conditions (very high air flow rates), the liquid surface becomes irregular, fluid constrictions may appear, and also multiple scattering of light from the liquid core is possible. Thus, the liquid core does not act like a perfect guide for the light in such cases.[31] However, since shorter liquid core

can be successfully illuminated by the OC technique, its application is still advantageous in comparison to the shadowgraphy technique.

The LIF images from the OC technique are processed to measure the instantaneous breakup length of the liquid jet (L) as shown in Figure 3. For this purpose, the average fluorescent intensity of each row of an image is calculated, which reduces the downstream of the nozzle exit (Figure 3). The axial location where it is below a threshold value identifies the jet breakup point, and the corresponding axial distance

from the nozzle exit measures the breakup length. The threshold value is decided such that close to the breakup point, there is sharp reduction in the intensity values. In the present case, this threshold value for an image was set to be 8% of the fluorescent intensity at the nozzle exit. This way the thresholding intensity is not constant and varies with the image under consideration. Thus, the technique is not sensitive to shot-to-shot variation in the power of the laser.[13] For each flow condition, the mean jet breakup length ($\bar{L}$) is calculated. Also, the fluctuations of the jet breakup length ($l = L - \bar{L}$) are determined and the corresponding root mean square (rms) value, denoted as l_r, is calculated. For each experiment, sufficient LIF images are captured, which ensured statistical convergence. A sensitivity analysis was carried out to examine the influence of the choice of the thresholding on breakup length measurement. It is found that increasing the threshold two times results in the reduction of $\bar{L}$ and l_r by 10% and 15%, respectively, while reducing the threshold to half of the selected value increases $\bar{L}$ and l_r by 15% and 20% respectively. However, the overall trend of either $\bar{L}$ or l_r with respect to We_g or M was found to remain unchanged. This ensures reliability of the employed image processing method.

We note here that the OC technique is suitable for imaging specifically the liquid core region during the primary jet breakup. In addition, due to low repetition rate of the employed laser in our experiments, the time-varying characteristics of the jet breakup process cannot be studied. Thus, in order to examine the jet instabilities during the breakup processes, high speed shadowgraph images were also captured. For this purpose, the spray was back-illuminated with an LED lamp. A Photron Fastcam Mini UX 100 camera was used for the visualization of the primary breakup process of the liquid jet. The images were acquired at the rate of 5000 frames per second (fps) for the flow conditions 1, 2 and 3 as shown in Table 1 and at 10,240 fps for the rest of the flow conditions. The image resolution was about 48 μm/pixel. The frame rate of image acquisition was higher for higher air flow rates and selected such that the time-resolved imaging of the jet breakup process was always ensured. For all cases, the camera exposure time of image acquisition was 5 μs, which is smaller than the minimum time scale of the air flow at the atomizer exit (corresponding to the maximum air flow rate considered in the present experiments). This ensured that the shadowgraph images can be safely assumed to be "instantaneous".

2.4. POD

The POD is a powerful mathematical tool for data analysis. POD essentially describes a given statistical ensemble with a minimum number of basis functions or deterministic modes. The literature on the application of POD for image analysis is already rich. In fact, POD has become a standard tool for image analysis for liquid jet/sheet atomization studies, and several research works have been reported in this area.[32–36] Hence, only a brief overview on POD is presented below. In the present work, the POD modes were calculated following the method of snapshots described by Sirovich.[37,38]

Let 'I_i' represents the intensity of an instantaneous image corresponding to i^{th} time instant. The intensity is spatially described over Q data points for each image. The POD of an ensemble of such images (with P number of sample images) leads to extraction of the spatial modes, $\phi_j(x)$ such that any image I_i can be expressed as a linear summation of the modes according to the following equation

$$I_i(x, t) = \sum_{j=1}^{r} a_{ij}(t)\sqrt{\lambda_j}\phi_j(x) \tag{4}$$

where 'x' and 't' are the independent variables denoting space and time respectively, $i = 1$ to P, $j = 1$ to r and $r < P$. $\phi_j(x)$s are the orthogonal eigenvectors, which are the spatial POD modes as mentioned earlier and λ_js are the corresponding eigen values. The eigen values are arranged in a decreasing manner ($\lambda_1 > \lambda_2 > \lambda_3 \ldots$) such that the eigen contribution ($\lambda_j/\sum\lambda_j$) for the first mode, i.e. ϕ_1 is the maximum, followed by the eigen contribution of the second mode, i.e. ϕ_2 and so on. $a_{ij}(t)$ are the temporal coefficients of a mode $\phi_j(x)$ A POD mode essentially represents an ensemble averaged feature of the whole ensemble, while the corresponding coefficients ($\sqrt{\lambda_j}a_{1j}, \sqrt{\lambda_j}a_{2j}\ldots.\sqrt{\lambda_j}a_{rj}$) indicate it's "weight" at different time instants $i = 1, 2,\ldots, P$, respectively. The power of POD lies in the fact that number of modes required to describe an image is the minimum, in other words, 'r' is the minimum so that the first few modes capture the most important spatial features of the flow.

From equation (4) the mean image ($\bar{I}(x)$) can be expressed as

$$\bar{I}(x) = \sum_{j=1}^{r} \alpha_j\sqrt{\lambda_j}\phi_j(x)$$
$$= \alpha_1\sqrt{\lambda_1}\phi_1(x) + \alpha_2\sqrt{\lambda_2}\phi_2(x) + \ldots.. \tag{5}$$

where $\bar{I}(x)$ is the mean image, and $\alpha_j (= \bar{a}_{ij})$ is the average of coefficients for mode $\phi_j(x)$.

Thus, if $\alpha_1\sqrt{\lambda_1} \gg \alpha_j\sqrt{\lambda_j}$ for $j = 2$ to r

$$\bar{I}(x) \approx \alpha_1\sqrt{\lambda_1}\phi_1(x) \qquad (6)$$

Hence, in such case, the first mode can be assumed to represent the mean image. This leads to

$$\sum_{j=2}^{r} \alpha_j\sqrt{\lambda_j}\phi_j(x) \approx 0 \Rightarrow \bar{a}_{ij} \approx 0 \quad \text{for } j = 2 \text{ to } r \qquad (7)$$

Hence, for the above case, the higher POD modes (second mode onwards) are indicative of the fluctuations relative to the mean and represent the dynamic features.

3. Results and discussion

3.1. Modes of liquid jet breakup in the air-blast atomizer

Figure 4 shows some instantaneous shadowgraph images of the liquid jet for four different operating flow conditions as examples. According to the morphological classification of disintegrating coaxial air-water jets based on the $We_g - Re_l$ map described in the literature, the jet breakup mode in the current experiments ($3000 < Re_l < 5000$ and $80 < We_g < 300$) falls into the fiber breakup regime[14] or either membrane or fiber breakup regime.[9] While, this is in good agreement with our shadowgraph visualization for the upper range of We_g in our experiments(Figure 4(c) and (d)), for the
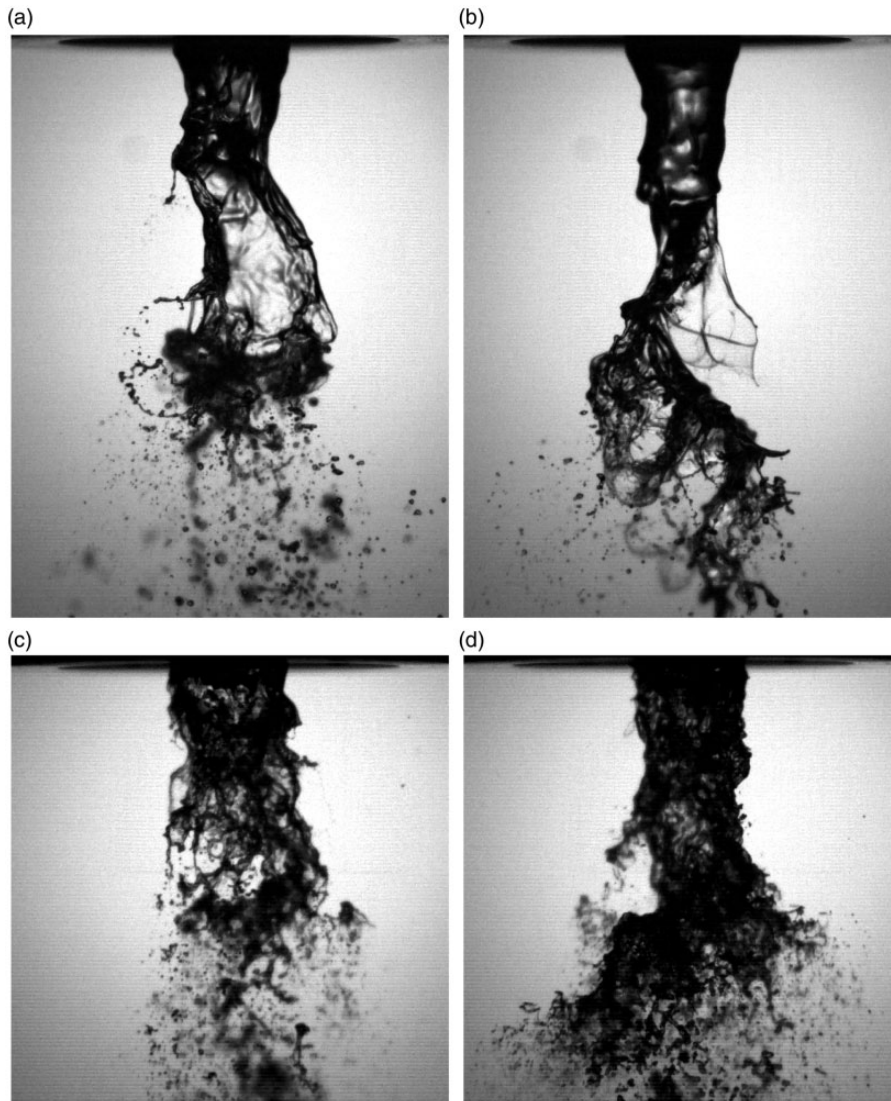

Figure 4. Shadowgraph images of the liquid jet breakup for four different operating conditions of the atomizer, (a) $U_l = 0.9$ m/s, $U_g = 42.1$ m/s, $We_g = 83.5$ and $M = 2.4$, (b) $U_l = 1.4$ m/s, $U_g = 42.1$ m/s, $We_g = 81.6$ and $M = 1.1$, (c) $U_l = 0.9$ m/s, $U_g = 78.6$ m/s, $We_g = 297.2$ and $M = 8.3$ and (d) $U_l = 1.4$ m/s, $U_g = 78.6$ m/s, $We_g = 293.6$ and $M = 3.7$.

low range of We_g (Figure 4(a) and (b)), both membrane breakup and fiber breakup are simultaneously observed. We note that the consequence of the differences in the nozzle geometry in the above works and the present case has not been considered in the above comparison. Recently, Zhao et al.[8] analyzed the influence of atomizer exit area ratio on the breakup morphology of the water–air jets. Following the breakup morphology suggested by these authors based on a modified $M - We_g$ map (which accounts for the exit area ratio), it is found that for the low range of We_g, the jet breakup mode is within the membrane-fiber breakup regime, which is considered as the transition breakup regime between the bag-type and fiber-type breakup mode of the liquid jet.[8] Formation of fiber and their peeling off the main liquid core are prominent for the upper range of We_g (Figure 4(c) and (d)). When the liquid flow rate is higher for the same air flow rate, the liquid core is longer and tends to be sinusoidal.

Figure 5 shows some instantaneous images of the liquid jet breakup measured by the OC technique for the same operating flow conditions as in Figure 4. Note that unlike the shadowgraph images, the OC images show only the unbroken liquid core region, while the detached liquid mass in the downstream region is not visible. Also, in contrast to the shadowgraph images, the liquid–air interface is sharp and identifying the breakup point is less ambiguous. The instantaneous images in Figure 5 also indicate the mean breakup length identified by the dotted horizontal lines. It can be observed that for a given injector operating condition even when the air and liquid flow rates at the atomizer inlet are constant, the liquid intact region (i.e. the axial distance from the nozzle exit up to the location where the jet diameter remains nearly same as the initial diameter at the nozzle exit) as well as the overall structure of the jet core vary significantly from one-time instant to other. Also, for all flow conditions, the wavelength of the interface instability is different at different time instants, and the liquid core length is sometimes larger or smaller relative to the mean breakup length. In addition, the jet is observed to flap to either side of the jet axis (Figure 5). Further downstream of the injector exit, such unsteadiness can lead to spatial and temporal fluctuations of liquid mass and volume flux, which influence the ability of the liquid fuel to react and release heat and are important for the stability and extinction of the flames.[39]

3.2. Characterization of liquid jet breakup length

3.2.1. Mean breakup length.
Figure 6(a) presents the trend of the normalized mean jet breakup length ($\bar{L}/D_l$) with respect to We_g for different liquid jet Reynolds number, Re_l. The error bars indicate the

statistical uncertainty with 95% confidence interval. The mean breakup length is typically three to six times the liquid jet diameter at the atomizer exit. As expected, the mean breakup length decreases for higher air flow rates and the same liquid flow rate, and increases with Re_l when the air flow rate is held constant. Thus, both We_g and Re_l are required to describe the jet breakup length. In contrast, as shown in Figure 6(b), a monotonic decreasing trend for the mean breakup length is observed for the higher momentum flux ratio, M. Earlier research works[1,5,12,26] also reported that the mean jet breakup length can be described by a single parameter, i.e. M. The correlations for the mean breakup length were obtained by curve fitting on the experimental data in Figure 6(a) and (b). The error in the curve fitting is within 8%. Table 2 presents the comparison of the present experimental correlations with those from the previous studies (which are based on shadowgraph measurements). In general, the overall trends of $\bar{L}$ versus We_g or M in the present study are in good agreement with the literature as similar power law relations are obtained (Table 2). However, in comparison to the earlier studies, in the present case, the coefficients and the exponents in the correlations are smaller and the measured mean breakup length is consistently lower. Charalampous et al.[13] have also reported similar observations based on their jet breakup length measurement by the OC technique and attributed this to the overestimation of jet breakup length in the shadowgraph image evaluation, as a result of hindrance caused by of the products of atomization.

3.2.2. Fluctuations of jet breakup length.
According to the earlier works using similar coaxial atomizer as ours, it has been observed that the Sauter mean diameter (SMD) of the spray droplets is inversely proportional to the velocity ratio, U_g/U_l,[3,28] while the mean jet breakup length is inversely proportional to the momentum flux ratio ($= U_g^2/U_l^2$). This means the shorter mean breakup length corresponds to smaller average droplet size. Thus, the mean jet breakup length carries the signature of the quality of atomization, and the variations in the instantaneous jet breakup length may correspond to the fluctuations of the size and number distribution of the spray droplets downstream of the atomizer. Hence, the fluctuations of jet breakup length must be characterized and the atomizer operating conditions for which the fluctuations are important relative to the characteristic jet breakup length must be identified.

Figure 7 presents the histograms of the normalized fluctuations of jet breakup length ($l/\bar{L}$) for the same flow conditions as in Figures 4 and 5. The histograms indicate that for any flow condition, the jet breakup
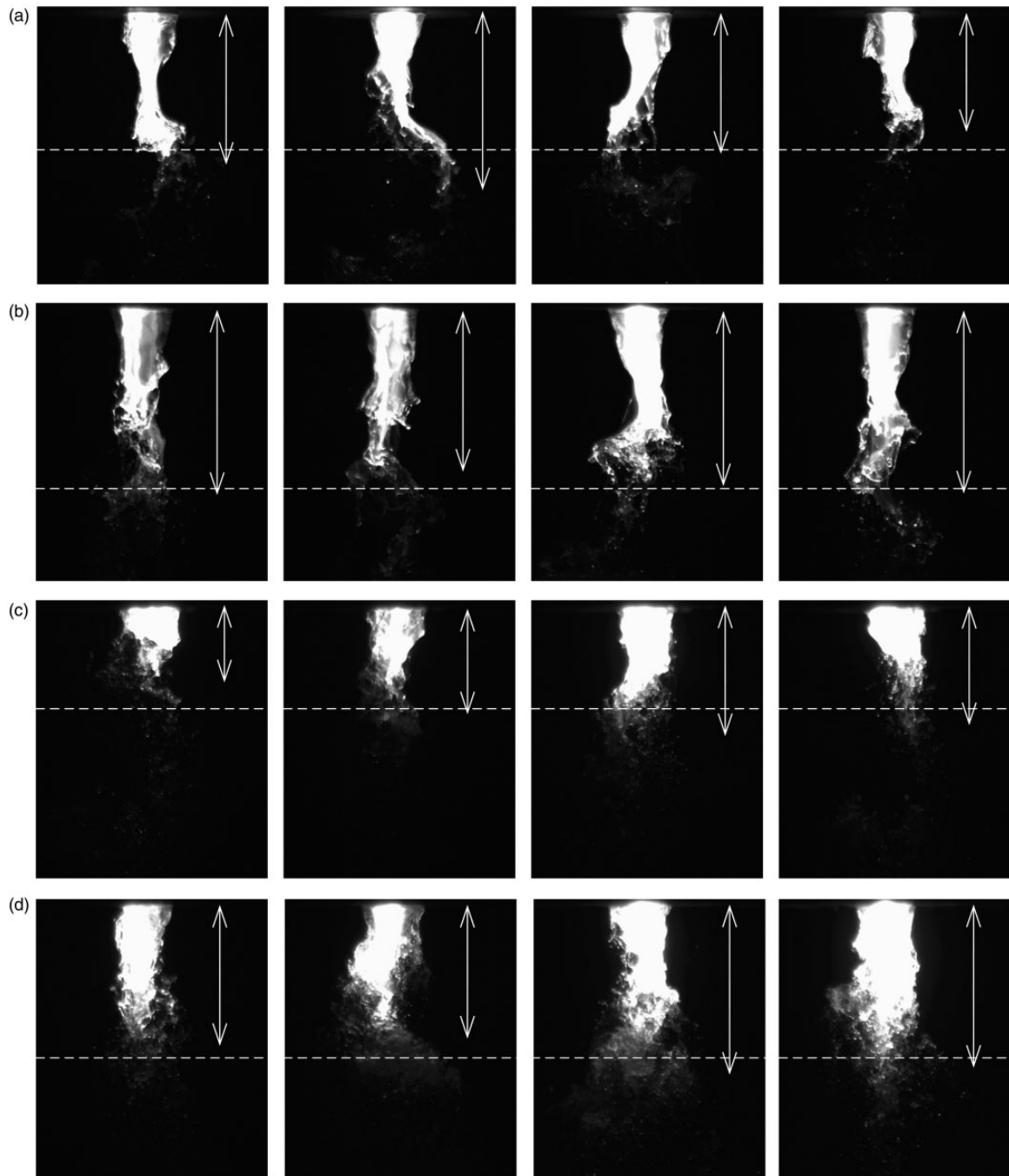
Figure 5. Instantaneous OC images for the same operating flow conditions of the atomizer as in Figure 4. The images highlight the temporal variation of the structure of the liquid core region. In each image, the arrow indicates the instantaneous breakup length, while the dashed line depicts the mean liquid jet breakup length. (a) $U_l = 0.9$ m/s, $U_g = 42.1$ m/s, $We_g = 83.5$ and $M = 2.4$, (b) $U_l = 1.4$ m/s, $U_g = 42.1$ m/s, $We_g = 81.6$ and $M = 1.1$, (c) $U_l = 0.9$ m/s, $U_g = 78.6$ m/s, $We_g = 297.2$ and $M = 8.3$ and (d) $U_l = 1.4$ m/s, $U_g = 78.6$ m/s, $We_g = 293.6$ and $M = 3.7$.

length is indeed not unique and may vary considerably. The fluctuations can be as large as 40% of the mean breakup length. Since the mean breakup length varies in the range $3D_l - 6D_l$ for the considered atomizer operating conditions. This means that the maximum fluctuation of the jet core length is about one liquid jet diameter.

Figure 8(a) shows the variation of the rms of the fluctuations of the instantaneous breakup length normalized with the mean breakup length (i.e. $l_r/\bar{L}$) with
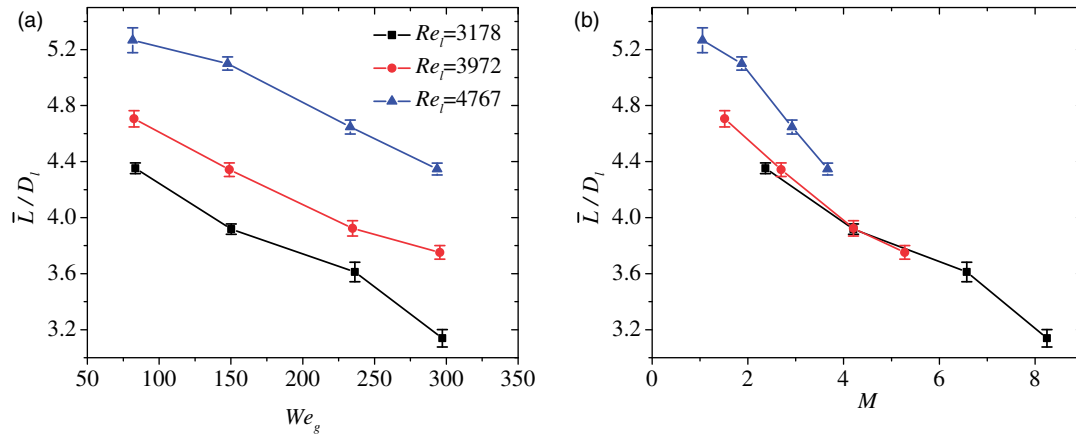
Figure 6. Normalized mean breakup length ($\bar{L}/D_l$) versus (a) We_g and (b) M, for different Re_l.

Table 2. Comparison of the experimental correlations for the mean jet breakup length in coaxial air-blast atomization.

Researchers	Breakup length correlation	Operating conditions
Eroglu et al.[4]	$\frac{\bar{L}}{D_l} = 0.66 We_g^{-0.4} Re_l^{0.6}$	$Re_l = $ 1100–18,000, $We_g = $ 13–267
Leroux et al.[12]	$\frac{L}{D_l} = \frac{10}{M^{0.3}}$	$Re_l = $ 45–1000, $We_g = $ 1–1000 and $M = $ 0.17–60
Zhao et al.[8]	$\frac{L}{D_l} = 5.2 \left(\frac{A_l}{A_g}\right)^{-0.17} M^{-0.28}$	$Re_l = $ 783–35,000, $We_g = $ 8.8–455 and $M = $ 0.011–620
Present study	$\frac{\bar{L}}{D_l} = 0.27 We_g^{-0.18} Re_l^{0.44}$	$Re_l = $ 3000–5000, $We_g = $ 80–300 and $M = $ 1.1–8.3
	$\frac{L}{D_l} = \frac{5.45}{M^{0.22}}$	

Note: A_l and A_g are the cross-sectional area for the liquid and air flow, receptively, at the exit of the atomizer. In the present study, A_l/A_g is 0.048. Incorporating this value in the correlation by Zhao et al.[8] following equation is obtained: $\bar{L}/D_l = 8.71 M^{-0.28}$.

respect to We_g. It is observed that for larger Re_l, the breakup length fluctuations relative to mean is about 10% for the considered range of We_g. However, when Re_l is lower ($Re_l = 3178$), the ratio is higher implying higher unsteadiness in the jet breakup process. Figure 8(b) shows $l_r/\bar{L}$ versus the momentum flux ratio, M. Similar to the mean breakup length, it seems the breakup length fluctuations can also be uniquely characterized with M. However, the trend is non-monotonic unlike the $\bar{L}/D_l$ versus M plot as shown in Figure 6(b). Figure 8 shows that when Re_l is low, the fluctuations of the breakup length show a monotonic increasing trend with the gas phase velocity indicating higher unsteadiness. However, for liquid Re_l, as the gas velocity is made higher, the fluctuations of the breakup length initially decrease and then increase. Interestingly, the minimum fluctuations are observed for M around 3 and We_g around 150. While for higher M, the higher unsteadiness in the jet breakup process is expected, we are unable to explain at present the opposite effect for large Re_l. Possibly, more experiments for wider range of M are required to explain the observed minimum in the above figure. But as M is increased, it is found that $l_r/\bar{L}$ increases monotonically. The ratio is about 20% for the highest M considered in the present experiments ($We_g = 297.2$ and $M = 8.3$)

indicating that the vertical fluctuation in breakup length is enhanced at high momentum flux ratio.

3.3. POD analysis of OC images

In order to capture the dynamics of the liquid jet breakup in greater detail, POD analysis of the OC images was carried out following the method described in the section 2.4. The POD results corresponding to the four operating flow conditions (same as in Figures 4 and 5) are presented in Figure 9 which depicts the first three POD modes for each case. The eigen contributions of the POD modes ($= \lambda_j / \sum \lambda_j$), which signify the energy content of the modes, are shown below in the respective modes. Figure 9 also shows the mean OC images for the considered flow conditions. The numerical values in each mode are normalized with respect to the corresponding maximum value such that the scale for the first mode is in the range of $0 - 1$, and the scale for the second and third modes is in the range of $-1 - 1$. It can be observed in Figure 9 that for all the cases, the first POD mode is qualitatively much similar to the mean image. In addition, the axial location (measured from the injector exit) where the numerical value within the first POD mode is about 10% of the value at the injector exit, is close to the mean breakup length
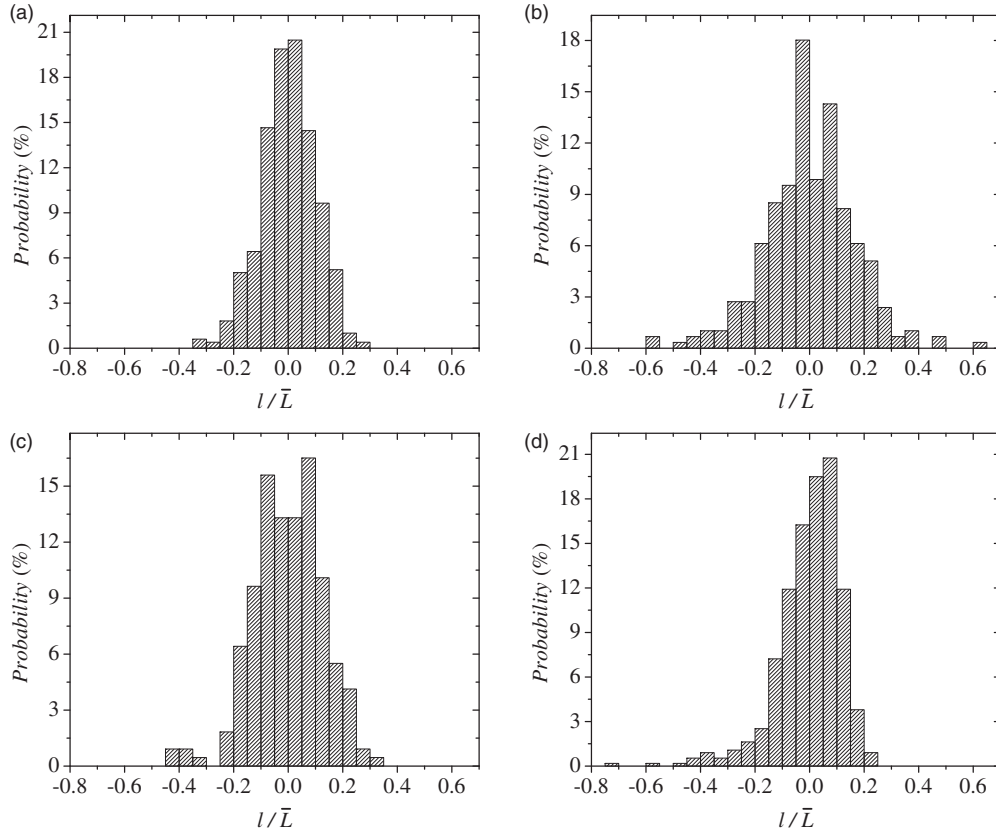
Figure 7. Histogram of normalized fluctuations of jet breakup length ($l/\bar{L}$) for the same atomizer operating conditions as in Figure 4. (a) $U_l = 0.9$ m/s, $U_g = 42.1$ m/s, $We_g = 83.5$ and $M = 2.4$, (b) $U_l = 0.9$ m/s, $U_g = 78.6$ m/s, $We_g = 297.2$ and $M = 8.3$, (c) $U_l = 1.4$ m/s, $U_g = 42.1$ m/s, $We_g = 81.6$ and $M = 1.1$ and (d) $U_l = 1.4$ m/s, $U_g = 78.6$ m/s, $We_g = 293.6$ and $M = 3.7$.
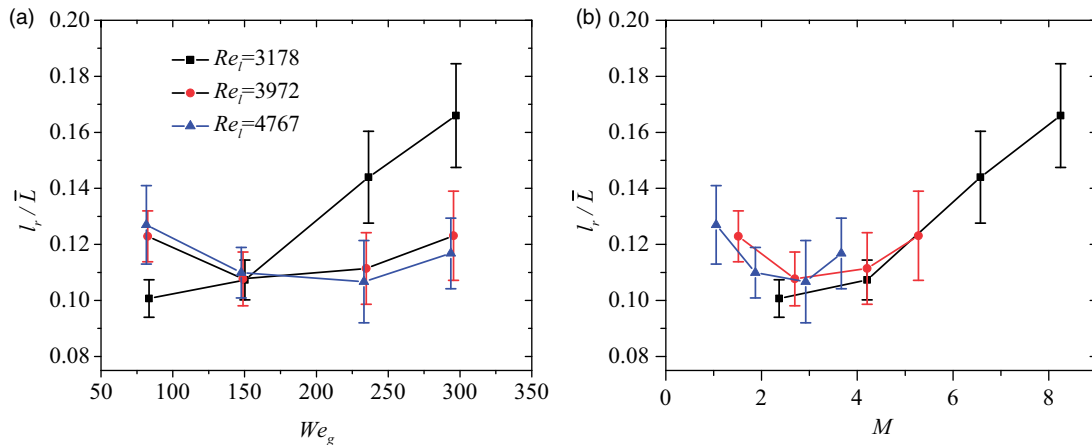

Figure 8. Normalized standard deviation of jet breakup length ($l_r/\bar{L}$) versus (a) We_g and (b) M, for different Re_l.

measured by the OC technique based on the thresholding of 8% as explained in the section 2.3. The similarity between the first POD mode and the mean OC image can be explained on the basis of the significant eigen contribution (about 80%) of the same mode for all operating conditions of the atomizer. Since for all the flow conditions, the average of the coefficients of the first mode is found to be much larger than those for the rest of the modes, i.e. $\alpha_1 \sqrt{\lambda_1} \gg \alpha_j \sqrt{\lambda_j}$ for $j \geq 2$ and the average coefficients for higher modes (second mode onwards) are close to zero ($\alpha_j \approx 0$) : $j > 2$, hence as per equation (6), the first mode can be assumed to
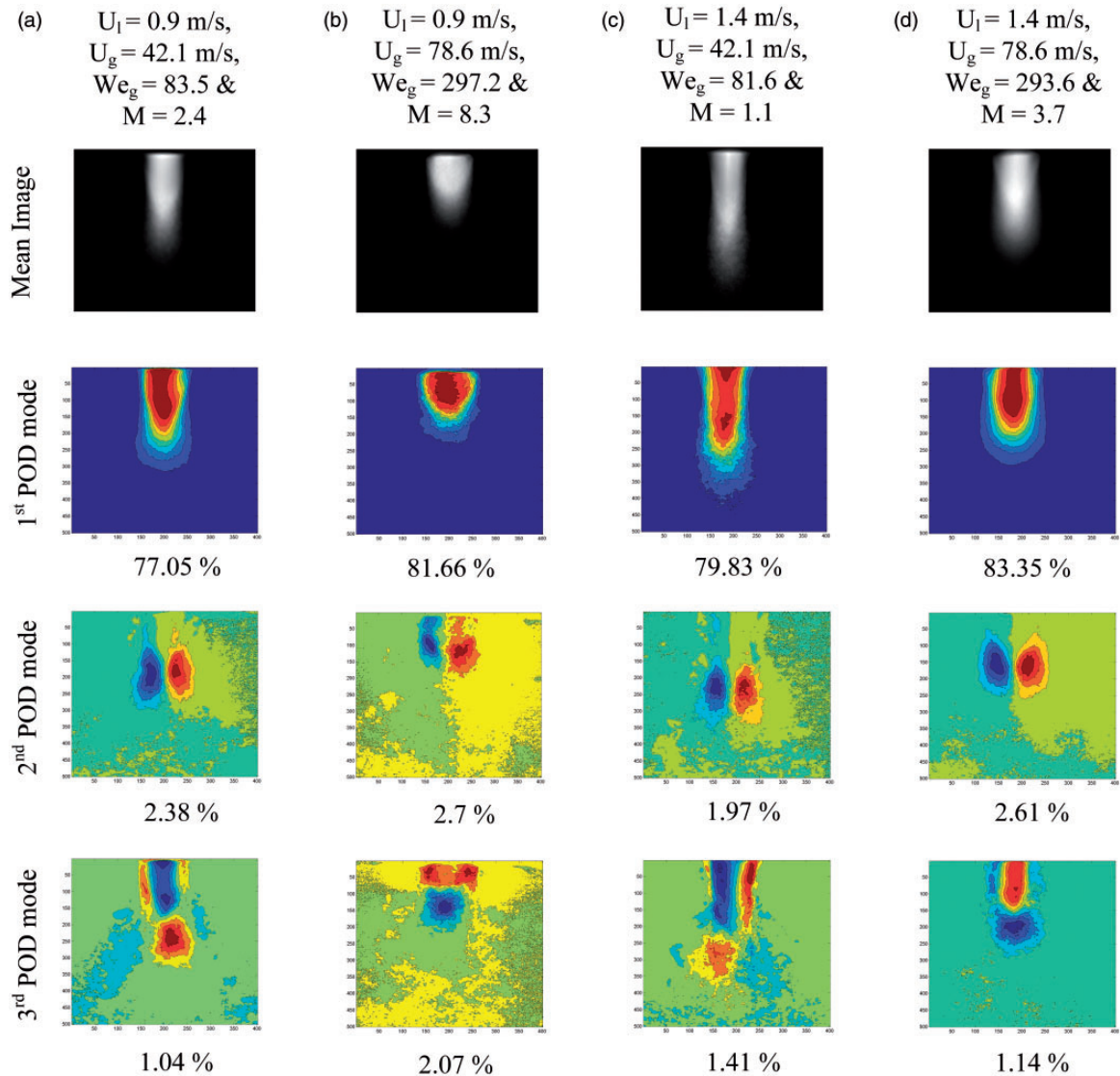
Figure 9. The mean image and the spatial POD modes for the same atomizer operating flow conditions as in Figure 4. The eigen contributions appear below each POD modes. The colorbar (blue-red) indicates the range $0 - 1$ for the first POD mode, and $-1 - 1$ for the second and third POD modes.

represent the average characteristics of the liquid core region and the rest of the modes characterizes the unsteadiness in the jet breakup process. Note that in Figure 9, the eigen contribution of the first POD mode is higher when U_g is higher at the same U_l, for example, compare Figure 9(a) and (b) or Figure 9(c) and (d). This is usually unexpected since this suggests reduction in the jet unsteadiness for higher gas velocity while the liquid velocity is held constant. However, such comparisons are not plausible since the eigen contribution of the first mode depends on the degree of spatial variability present in the images. The lower is the spatial variability in the images, the higher is the eigen contribution of the first mode. In other words, the eigen contribution of the first mode is 100% for the hypothetical

case for which the jet core image does not vary with time. Since the spatial resolution of the OC images is the same for all operating flow conditions, thus the small scale variations (which are prominent when the liquid–air relative velocity is higher) are spatially averaged, and, so, the eigen contribution is higher. Hence, the higher eigen contribution of the first mode for higher air flow rate at the same liquid flow rate as observed in Figure 9 is due to the spatial resolution in the images rather than the flow dynamics. However, in the present work, the focus is on the trend of the eigen contribution of second and third POD mode with respect to the momentum flux ratio. It is reasonable to compare the eigen contributions of the second and third modes for different flow conditions since such

mode represents the fluctuations about the mean image and represents specific dynamic features. In fact, we verified the above by reducing the spatial resolution (binning the OC images), and as a consequence, the eigen contribution of the first mode was found to be higher, while no significant variation was observed for the next two modes.

The eigen contribution of the second POD mode is about (2–3)% for all atomizer operating conditions. This mode shows the presence of a positive and a negative lobe located away from the atomizer exit and on either side of the atomizer axis. As mentioned earlier, the average of the modal coefficients is nearly equal to zero, i.e. $\sum a_{i2} \approx 0$. Hence, depending on the sign of the coefficients (a_{i2}) for the second POD mode being positive or negative, the mode indicates the presence of the jet core on either side of the axis of the atomizer. It was also found that for any operating flow condition, the axial location of the center of either the positive or the negative lobe in the second mode is close to the mean jet breakup length for that flow condition. The above results point out that the second mode represents the lateral oscillation of the tail end of the jet indicating the flapping instability of the jet. Also, the jet flapping on either side of the axis of the injector is equally probable. In fact, the jet flaps around the spray axis, the symmetry in the second mode is due to the two-dimensional imaging in the present experiments. Also, interestingly, the topology of the second POD mode is very similar for all the cases (including those not shown in Figure 9) implying that the flapping instability is inevitable for all the operating conditions of the atomizer. However, the eigen contribution of the second mode is proportional to the momentum flux ratio, M as shown in Figure 10(a). Also, it increases sharply with respect to M when the jet Reynolds number is high.

Since the second POD mode represents the lateral displacement of the jet, it does not contribute to the axial variation of the jet core length. However, the third POD mode shows that the modal values are alternately negative and positive along the axis of the atomizer, and also $\sum a_{i3} \approx 0$. This suggests that the third mode represents the fluctuations of the jet breakup length. The variation of the eigen contribution of the third mode with respect to M is shown in Figure 10(b) which is similar to the plot of $l_r/\bar{L}$ versus M in Figure 8(b). Also, similar to the second POD mode, the basic topology presented by the third mode was found to be similar for all operating flow conditions in spite of the large differences in the momentum flux ratios and the mean breakup lengths.

The higher POD modes (fourth mode onwards) show small scale variations in the jet core structure, which is not only due to the jet dynamics but may also result, for example, from the differences in the imaging due to shot-to-shot variation in the laser power or background intensity variation etc. Moreover, the eigen contributions of those modes are less than 1%. Hence, those modes are not presented here. Also, it was found that unlike the second and third POD modes, the topology of those modes is not unique, rather varies for different operating flow conditions. It can be observed in Figure 9 that the background intensity is close to zero in the first POD mode, which corresponds to the mean image. The higher modes represent the fluctuations of the intensity around the mean. Hence, some fluctuations of the background intensity are also captured in the second and third POD modes. However, the modal values corresponding to those regions are close to zero and much smaller than the values at the region of interest, i.e. positive and negative lobes representing jet flapping in
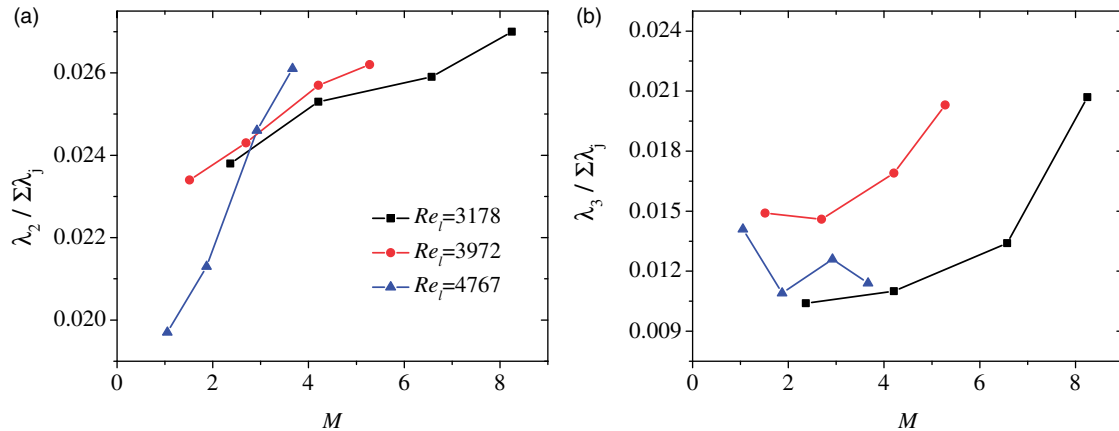

Figure 10. Eigen contributions of the POD modes ($\lambda_j / \sum \lambda_j$) versus momentum flux ratio (M) for (a) second mode and (b) third mode.

the second mode and vertical breakup length fluctuation in the third mode. Hence, the background features in those modes are not important.

3.4. Characterization of liquid jet instabilities using high-speed imaging

As mentioned earlier, due to low repetition rate of the laser, the LIF images of the liquid core region in the OC technique are not time resolved. Hence, some important dynamic features of the liquid jet instability such as the jet flapping cannot be discerned in greater detail. Hence, high-speed shadow images of the jet breakup region close to the atomizer exit were captured for different injector operating conditions as outlined in Table 1. The amplitude and the frequency of the interfacial disturbances are characterized by temporal tracking of the liquid–air interface at two different axial locations ($z = D_l$ and $\bar{L} - D_l$) downstream of the atomizer exit as demonstrated in Figure 11 and explained below. The instantaneous right- and left- interface positions about the injector axis are denoted as y_R and y_L, respectively. It is noted here that, while at $z = D_l$, y_R and y_L are always positive and negative, respectively, at $z = \bar{L} - D_l$, y_R (or y_L) can be either positive or negative depending on the position of the right (or the left) interface relative to the injector axis. Thus, when the ratio y_L/y_R is close to '−1', the position of the interfaces is symmetrically located about the injector axis.

1. Measurement at $z = D_l$: The purpose here is to identify the frequency of the most unstable disturbance close to the atomizer exit. Figure 11 shows an example of the time-varying right interface position at $z = D_l$. It was found that $y_R \approx y_L$ such that the ratio y_L/y_R is close to '−1' as shown in Figure 12(a) indicating axis-symmetric disturbances close to the atomizer exit. Also, the power spectra for both y_L and y_R, obtained by taking Fast Fourier transforms (FFT) of the signals, are similar. This suggests that the peak amplitude in the power spectrum corresponds to the shear driven KH instability in agreement with Marmottant and Villermaux[24] and Matas and Cartellier,[26] who also reported similar results in their measurements close to the atomizer exit. The corresponding frequency is denoted as f_{KH}.

2. Measurement at $z = \bar{L} - D_l$: The purpose here is to identify the mechanisms of the jet instability in particular, the flapping instability, which has been found to be dominant near the jet breakup location[26] away from the atomizer exit. Thus, the time varying-liquid–air interface location downstream of the injector exit at $z = \bar{L} - D_l$ was considered. The selection of this location is justified since this corresponds to the axial locations of the center of the positive or negative lobes observed in the second POD mode, which represents the jet flapping as explained earlier. As observed in Figure 12(b), the histogram of the ratio y_L/y_R was found to be much broader and the ratio considerably deviates from '−1' signifying asymmetric location of the interface about the atomizer axis. Especially, the positive values of the ratio y_L/y_R indicate that both left and right interfaces
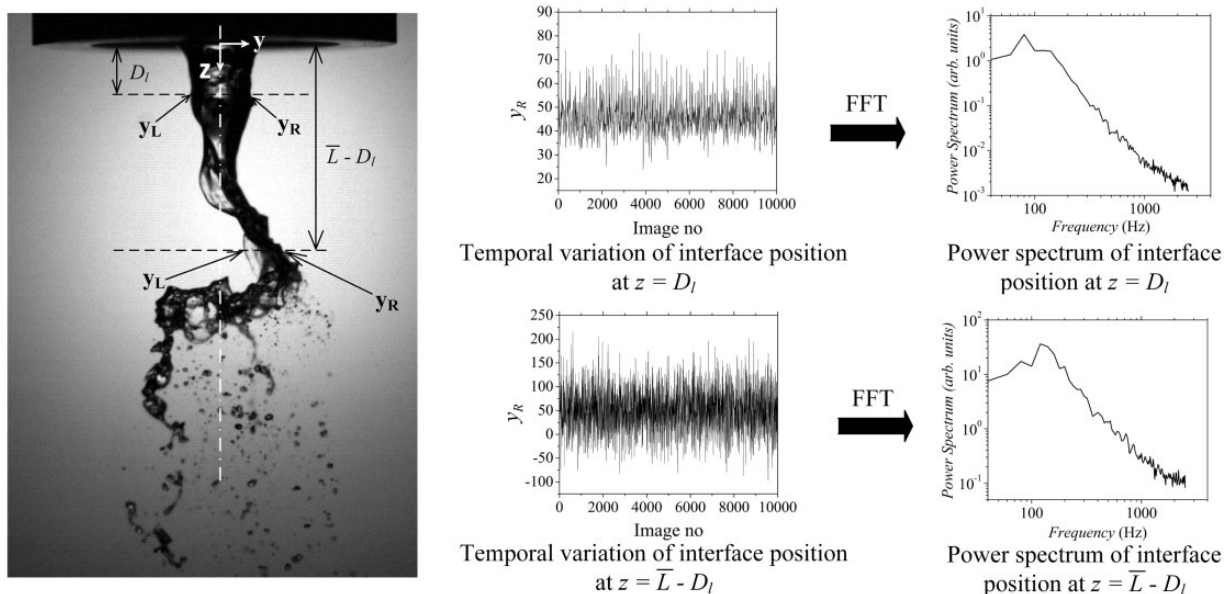

Figure 11. Method of characterization of jet instability at different axial location $z = D_l$ and $\bar{L} - D_l$ downstream of the atomizer exit.
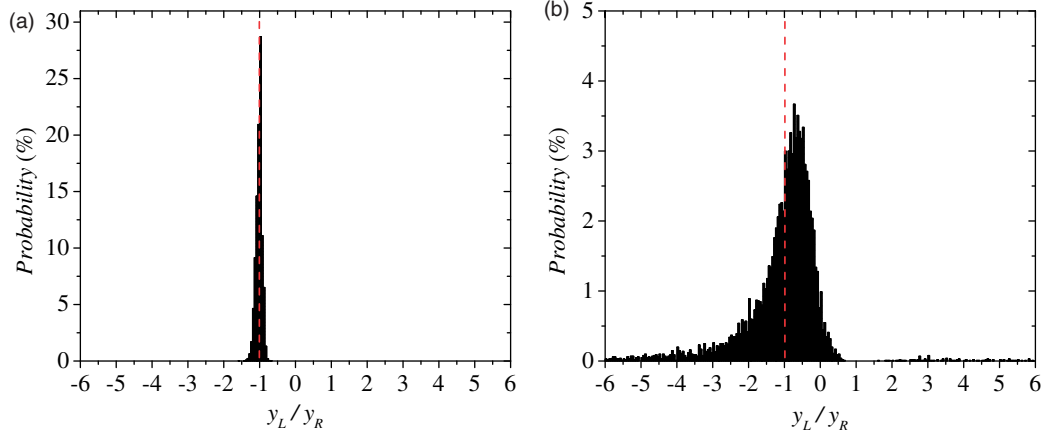
Figure 12. Histogram of the ratio of the left and the right interface location (y_L/y_R) for an axial distance $z =$ (a) D_l and (b) $\bar{L} - D_l$ for the flow condition 3 in Table 1 ($U_l = 1.4$ m/s, $U_g = 42.1$ m/s, $We_g = 81.6$ and $M = 1.1$).
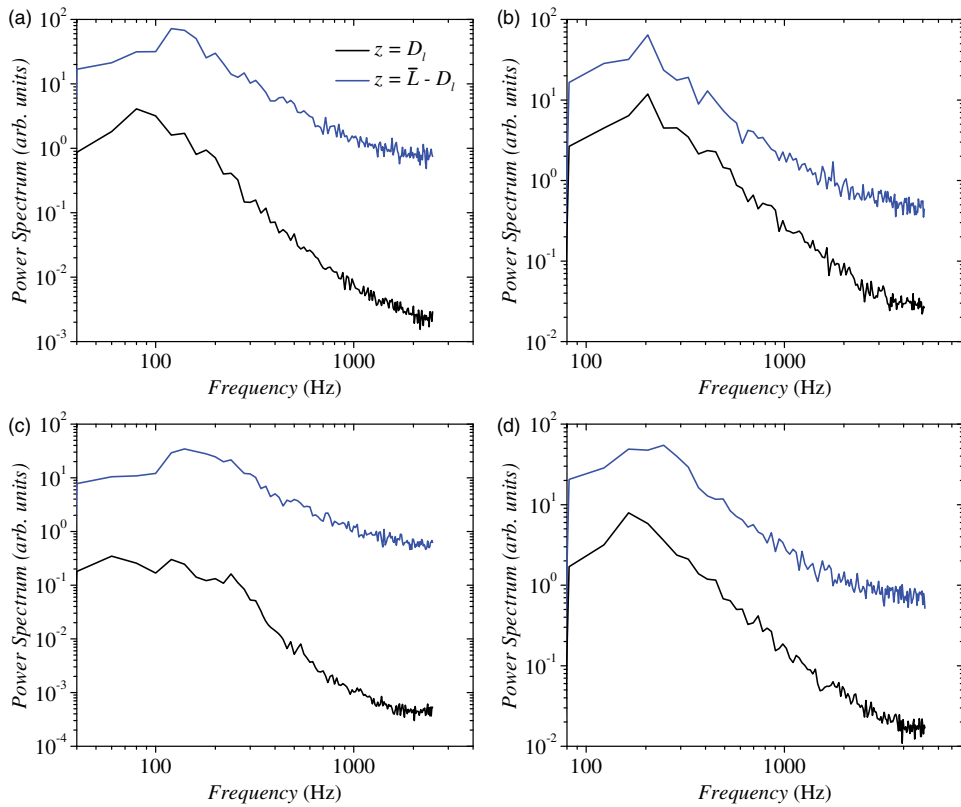

Figure 13. Comparison of the power spectrums of the right liquid–air interface location at $z = D_l$ and $\bar{L} - D_l$ for the atomizer operating flow condition same as in Figure 4. (a) $U_l = 0.9$ m/s, $U_g = 42.1$ m/s, $We_g = 83.5$ and $M = 2.4$, (b) $U_l = 0.9$ m/s, $U_g = 78.6$ m/s, $We_g = 297.2$ and $M = 8.3$, (c) $U_l = 1.4$ m/s, $U_g = 42.1$ m/s, $We_g = 81.6$ and $M = 1.1$ and (d) $U_l = 1.4$ m/s, $U_g = 78.6$ m/s, $We_g = 293.6$ and $M = 3.7$.

are on the same side of the injector axis (for example, see the shadowgraph image in Figure 11), which means flapping of the tail end of the jet. However, the power spectrums of both y_L and y_R were similar. The frequency corresponding to the maximum amplitude in the power spectrum

corresponds to the flapping instability of the jet and is denoted as f_{flap}.

Figure 13 compares the power spectrums of the right interface location (y_R) at $z = D_l$ and $\bar{L} - D_l$ for the four atomizer operating conditions for which the

shadowgraph images are shown in Figure 4. In order to filter out the high frequency noise from the signal corresponding to time-varying liquid–air interface location, similar to Matas et al.,[40] the signal was split into 20 segments and the average spectrum is obtained. The number of segments was decided as a trade-off between the frequency resolution and the signal conditioning. In the present case, the resolution of the measured frequency was 10 Hz for the images taken at 5000 fps, while it was about 20 Hz for the images taken at 10240 fps. In general, the amplitude of the spectrum is higher for the location away from the injector exit, where the deflection of the liquid–air interface is larger in comparison to the near nozzle location. Also, it is observed that the two spectrums are closer for higher momentum flux ratio. For the low momentum flux ratio ($M=1.1$), multiple peaks with nearly equal amplitude appear in the power spectrum especially for the near nozzle location at $z = D_l$. It was found that for any flow conditions, the power spectrum does not vary much when the axial location is varied in the range $z \pm D_l$.

Figure 14(a) shows the variation of f_{KH} with respect to the inlet gas velocity, U_g. It is observed that for the considered range of U_g and U_l, f_{KH} is proportional to U_g and weakly dependent on the liquid Reynolds number, Re_l. Thus, higher the gas velocity U_g, higher is the waviness on the liquid jet interface since the interfacial waves of smaller wavelength are formed. Lasheras et al.[1] found that the frequency of the disturbances close to the atomizer exit is proportional to U_g^2 and U_g depending on the liquid inlet flow being laminar and turbulent respectively (Re_l smaller and larger than about 2000). Since in the present case, $Re_l > 2000$, our results are in agreement with Lasheras et al.[1] In order to compare the time scale of the initial disturbances with the liquid flow time scale at the nozzle exit, the Strouhal number (St_l) is defined as below

$$St_l = \frac{f_{KH} D_l}{U_l} \tag{8}$$

Figure 14(b) shows that in general $St_l < 1$, and for low momentum flux ratios ($M < 2$), $St_l \approx 0.1$. Thus, the
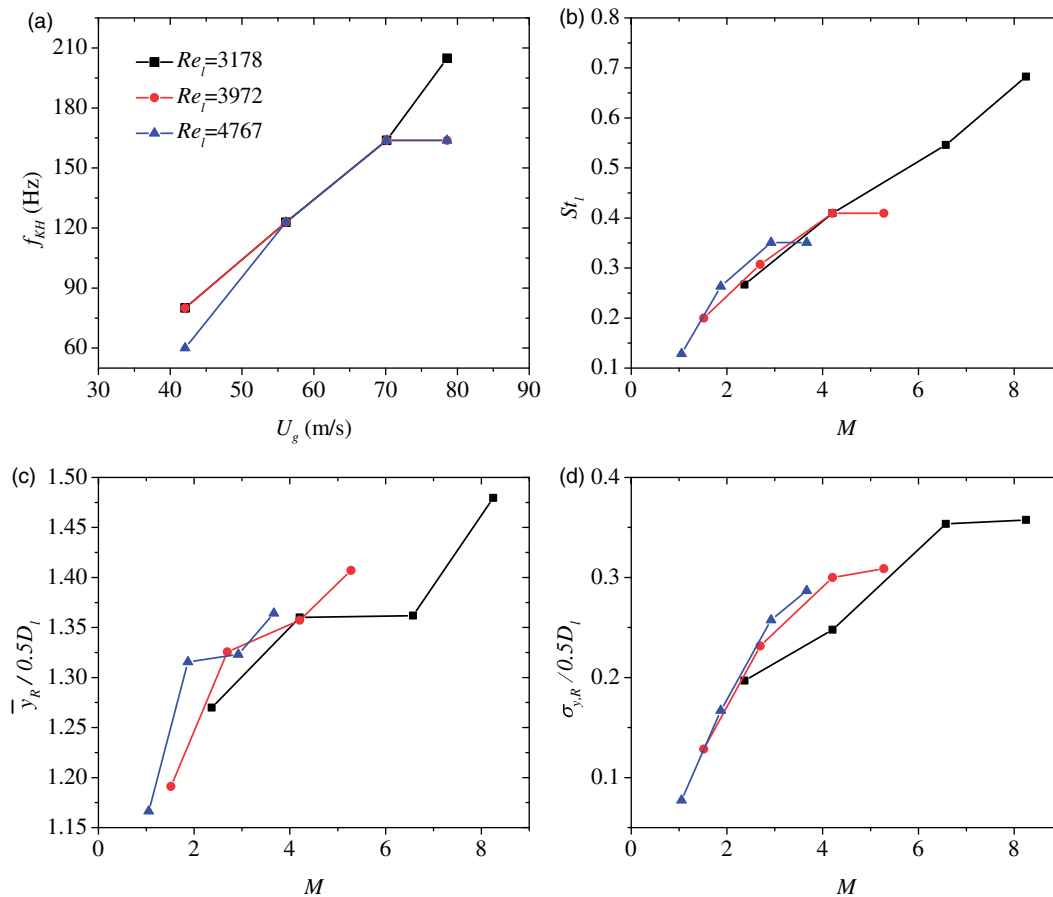

Figure 14. (a) f_{KH} vs. U_g, (b) St_w vs. M, (c) $\bar{y}_R/0.5D_l$ vs. M and (d) $\sigma_{yR}/0.5D_l$ vs. M, for axial location at $z = D_l$.

initial disturbances grow slowly in comparison to the liquid flow rate at the near nozzle location. This is possibly due to the liquid boundary layer developed within the central tube in the atomizer. At the nozzle exit and near the inner wall of the central tube, the liquid velocity is nearly zero. Thereafter, the liquid accelerates downstream due to interaction with the surrounding high-speed air flow. Figure 14(b) further shows that St_l is proportional to the momentum flux ratio, M. The Strouhal number approaches 'one' as M is higher since the liquid near the jet interface accelerates quickly such that the time scale of the instability and the liquid flow is of similar order. Earlier, Chigier and Dumouchel[41] identified the necessity to take into account, the velocity profile relaxes in the downstream of the injector exit. Thus, it is important to consider the effect due to the boundary layer in the fluids (which develop within the atomizer) in the analysis and simulation of the jet breakup process. Our experimental results are in good agreement with the above assertion. It is noted that the Strouhal number can also be defined based on the average gas velocity at the exit of the atomizer ($St = f_{KH}(D_o - D_i)/U_g$). In such case, its trend with respect to M (not shown here) is similar to Figure 14(b). However, the Strouhal number is much smaller and in addition, the influence of Re_l is higher in comparison to Figure 14(b).

Figure 14(c) and (d) presents the mean and the standard deviation of the right interface (denoted as $\bar{y}_R$ and $\sigma_{y,R}$, respectively) at location $z = D_l$ for different momentum flux ratios. Both quantities are normalized with the inlet jet radius $0.5D_l$. The mean interface location is proportional to M and depends weakly on the liquid jet Reynold number, Re_l. While $\bar{y}_R$ is nearly equal to the jet radius when the momentum flux ratio is low ($M \approx 1$) as expected, for higher M, the jet expands in the lateral direction. For example, the jet diameter increases by about 50% for $M \approx 8$. Also, a substantial increase in the fluctuations of the interface location is observed for higher M (Figure 14(d)) indicating the disturbances of larger amplitude. The radial expansion of the jet and the larger interface perturbations at higher momentum flux ratio is due to the existence of a gas cavity near the central region of the jet. The origin behind such gas cavity has been attributed to recirculation of the air flow.[1] In contrast to Figure 14(c), the measurements at $z = \bar{L} - D_l$ location (Figure 15(a)) indicate that though the mean interface location is proportional to M, it strongly depends on Re_l and the effect is significant when Re_l is higher. For example, for $Re_l = 4767$, the mean interface location was about two times the jet radius when the gas velocity is maximum (flow condition 12 in Table 1). The fluctuations of the interface location are observed to vary inversely with M (Figure 15(b)). This is again in

contrast to the results obtained for the near nozzle location at $z = D_l$ in Figure 14(d). However, the jet breakup length ($\bar{L}$) reduces for higher M, and the quantities $\bar{y}_R/\bar{L}$ and $\sigma_{y,R}/\bar{L}$ were found to be proportional to M and nearly independent of the Re_l (not shown here). At the axial position $z = \bar{L} - D_l$, the mean and the standard deviation of the interface location was, respectively, about 10–20% and 10% of $\bar{L}$. This means that a different scaling is necessary to describe the amplitude of the disturbances near the breakup point in comparison to the same at the near nozzle location. This is again in agreement with Chigier and Dumouchel[41] and suggests that a different mechanism of jet instability is in action downstream of the jet exit near the breakup location.

The disturbances generated near the nozzle exit grow further downstream of the injector exit leading to the breakup of the liquid jet. According to Matas and Cartellier,[26] when the liquid jet breakup length is larger than the potential core length of the annular gas flow, the liquid jet near the breakup point exhibits lateral oscillations with amplitude comparable to the inlet jet diameter at the atomizer exit. This leads to breakup of the liquid jet in to larger ligaments. The above authors termed it as the 'flapping' instability, which is different from the shear-driven KH instability. As the gas velocity is higher, the gas potential cone length increases[42] and the liquid jet breakup length decreases, which results in reduction of the amplitude of large scale oscillating waves. In the present experiments, the flapping frequency (f_{flap}) measured at $z = \bar{L} - D_l$ is found to be proportional to the gas velocity in agreement with Matas and Cartellier.[26] However, it is observed in Figure 15(c) that for higher gas velocity, f_{flap} is larger when the liquid Reynolds number is large ($Re_l = 4767$). Also in the plot f_{flap} versus M (not shown here), it was found that the rate of increase of the flapping frequency with respect to M is higher for the liquid flow with larger Reynolds number. This concurs with our earlier finding in Figure 10(a) which shows a sharp increase in the eigen contribution of the second POD mode (which depicts the jet flapping) for the highest Re_l. Thus, unlike the KH instability which is mostly governed by the gas flow velocity, the liquid flow rate additionally influences the flapping instability. The comparison of the frequencies of both instabilities is of interest. Figure 15(d) presents f_{flap}/f_{KH} for different momentum flux ratios. It can be observed that $f_{flap} > f_{KH}$ for low M, and the ratio is smaller and close to 'one' as M is higher. For the lowest momentum flux ratio ($M \approx 1$) in the present experiments, f_{flap} is more than two times of f_{KH}. This suggests that a different mechanism is responsible for the flapping instability of the jet. In their numerical study of a plane liquid sheet sheared
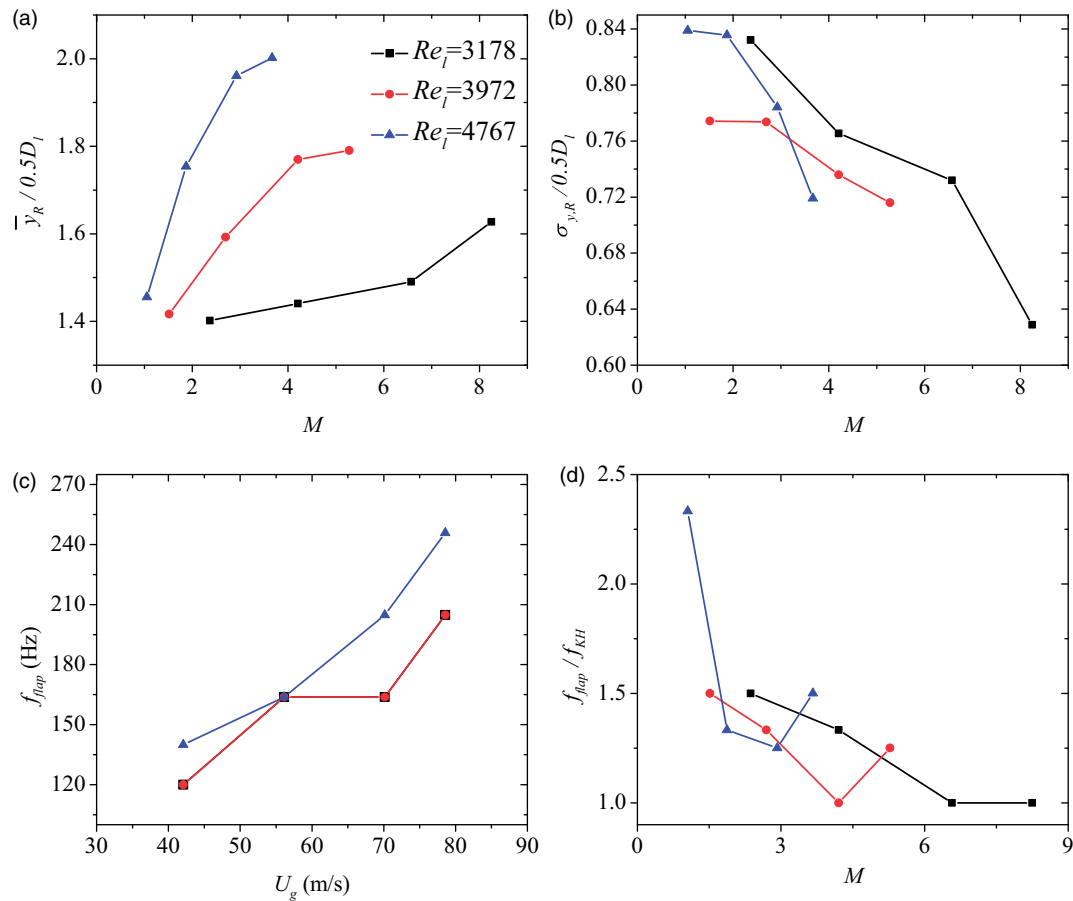
Figure 15. (a) $\bar{y}_R/0.5D_l$ vs. M, (b) $\sigma_{yR}/0.5D_l$ vs. M, (c) f_{flap} vs. U_g and (d) f_{flap}/f_{dist} vs. M, for axial location at $z = \bar{L} - D_l$.

by a high-speed stream, Odier et al.[27] identified that the coupling between the low pressure area on one side of the sheet (due to vortex detachment) and the high pressure area on the other side (as it acts as an obstacle for the high-speed stream) is responsible for the flapping of the liquid sheet. However, due to the differences in the geometric configuration of a coaxial jet and a sheet, there is no preferential orientation of the plane of the flapping of the jet (corresponding to the lateral oscillation of the jet) as in the case of the liquid sheet, since in the case of former, it may randomly change with time.[26] Thus, there is yet no general consensus if the same mechanisms for flapping of a liquid sheet are also responsible for the jet flapping. We note that in their experiments, Matas and Cartellier[26] found that the flapping frequency is smaller than the KH frequency. However, in their experiments, the ranges of gas and liquid velocities were lower as compared to our experiments. Also, the flapping frequency was measured at $10D_l$ location from the atomizer exit for all cases, while in our case, this location is according to the liquid jet breakup length corresponding to the operating flow condition of the atomizer.

We note that the initial turbulence intensity of the air flow, air recirculation at the nozzle exit and the shear layer due to interaction of the air flow with the ambient air, influence the jet instability and breakup of the liquid jet. For instance, the flapping of the jet is a large scale instability, which is expected to be governed by the energy containing large eddies of the air flow. However, any quantitative discussion on the above requires characterization of the air velocity in presence of the liquid jet, which has not been measured in the current experiments. Especially, planer measurement of velocity and vorticity fields of gas phase in the vicinity of the liquid jet can provide useful information on the dynamics of the jet breakup process. However, our current effort is in that direction.

4. Conclusions

The primary breakup of liquid jet in a coaxial air-blast atomizer was experimentally characterized with emphasis on the measurement of the fluctuations of the jet breakup length and the flapping instability. Such instabilities during the jet breakup process may cause

fluctuations of the spray characteristics further downstream. The atomizer was operated under atmospheric conditions for a range of momentum flux ratio (M: 1–8) and aerodynamic Weber number (We_g: 80–300), which correspond to membrane- and/or fiber breakup mode of the liquid jet breakup process. The OC technique was used to visualize the liquid core region during primary breakup of the liquid jet as well as to measure the instantaneous jet breakup length. The mean jet breakup length was found to follow a power law relation with M in agreement with the literature. The fluctuations of the jet breakup length (relative to the mean) was also measured and found to first decrease and then increase with M. The rms of the jet breakup length fluctuations was about 20% of the mean value for the highest momentum flux ratio ($M \approx 8$). These results are supported by the POD analysis of the OC images which indicated the fluctuations of the jet breakup length in the third POD mode for all operating conditions of the atomizer. In fact, the variation of the eigen contribution of the same mode with respect to M is similar to that for the rms of the breakup length fluctuations. Considering that the breakup length of the liquid jet is an important parameter, which signifies the atomization quality and is relevant to spray simulations, the consequence of the breakup length fluctuations must be considered in greater detail especially for high momentum flux ratios.

The amplitude and the frequency of the instabilities were measured based on the temporal measurement of the liquid–air interface in the high-speed shadowgraph images. The disturbances at one liquid jet diameter away from the atomizer exit was found to correspond to the KH instability, which was characterized by the symmetric distribution of the ratio of the left and right liquid–air interface locations (y_L/y_R) in the shadowgraph images. As a consequence of the boundary layer developed within the atomizer, the growth of the instability close to the injector is at a lower rate than the liquid flow velocity at the injector exit. Thus, in the present experiments, the Strouhal number based on the measured frequency of the KH instability (f_{KH}) is always less than 'one'. Further downstream of the injector exit and close to the jet breakup point, the distribution of y_L/y_R was asymmetric implying jet oscillations in the direction normal to the axis of the atomizer. This suggests the dominance of the flapping instability. This is further supported by the second POD mode of the OC images, which indicates a positive and a negative lobe on either side of the atomizer axis. In fact, interestingly, the topology represented by the second POD mode is same for all cases implying that the jet flapping is inevitable for the range of the atomizer operating conditions considered in the present experiments. Similar to f_{KH}, the frequency of the jet flapping (f_{flap}) is proportional to the inlet gas velocity (U_g). However, for low M, $f_{flap} > f_{KH}$ and the ratio is close to one as M is higher. While the amplitude and the frequency of the disturbances close to the nozzle exit are found to be governed by U_g and almost independent of the jet Reynolds number, Re_l, the lateral oscillation of the jet near the breakup point due to the jet flapping and the corresponding frequency are higher for larger Re_l.

Declaration of Conflicting Interests

Funding

ORCID iD

Srikrishna Sahu http://orcid.org/0000-0003-2684-5979

References

1. Lasheras J, Villermaux E and Hopfinger E. Break-up and atomization of a round water jet by a high-speed annular air jet. *J Fluid Mech* 1998; 357: 351–379.
2. Hoyt JW and Taylor JJ. Waves on water jets. *J Fluid Mech* 1977; 83: 119–127.
3. Lefebvre AH. *Atomization and sprays*. New York: Hemisphere Pub. Corp., 1989.
4. Eroglu H, Chigier N and Farago Z. Coaxial atomizer liquid intact lengths. *Physi Fluids A* 1991; 3: 303–308.
5. Engelbert C, Hardalupas Y and Whitelaw JH. Breakup phenomena in coaxial airblast atomizers. *Proc R Soc Lond A* 1995; 451: 189–229.
6. Lin S and Reitz R. Drop and spray formation from a liquid jet. *Ann Rev Fluid Mech* 1998; 30: 85–105.
7. Reitz R and Bracco F. Mechanism of atomization of a liquid jet. *Phys Fluids* 1982; 25: 1730–1742.
8. Zhao H, Liu HF, Tian XS, et al. Influence of atomizer exit area ratio on the breakup morphology of coaxial air and round water jets. *AIChE J* 2014; 60: 2335–2345.
9. Lasheras J and Hopfinger E. Liquid jet instability and atomization in a coaxial gas stream. *AnnRev Fluid Mech* 2000; 32: 275–308.
10. Woodward R, Burch R, Kuo KK, et al. Correlation of intact-liquid core length for coaxial injectors. In: *Proceedings of ICLASS*, Rouen, France, 18–22 July 1994, Volume 94, pp.105–112.
11. Porcheron E, Carreau JL, Le Visage D, et al. Effect of injection gas density on coaxial liquid jet atomization. *Atomizat Sprays* 2002; 12: 209–227.
12. Leroux B, Delabroy O and Lacas F. Experimental study of coaxial atomizers scaling. Part I: dense core zone. *Atomizat Sprays* 2007; 17: 381–407.
13. Charalampous G, Hardalupas Y and Taylor A. Novel technique for measurements of continuous liquid jet core in an atomizer. *AIAA J* 2009a; 47: 2605.

14. Chigier N and Farago Z. Morphological classification of disintegration of round liquid jets in a coaxial air stream. *Atomizat Sprays* 1992; 2: 137–153.

15. Chigier N and Reitz RD. Regimes of jet breakup and breakup mechanisms- physical aspects. *Recent Adv Spray Combust* 1996; 1: 109–135.

16. Charalampous G, Hardalupas Y and Taylor A. Structure of the continuous liquid jet core during coaxial air-blast atomisation. *Int J Spray Combust Dyn* 2009b; 1: 389–415.

17. Villermaux E. Mixing and spray formation in coaxial jets. *J Propul Power* 1998; 14: 807–817.

18. Dumouchel C. On the experimental investigation on primary atomization of liquid streams. *Exp Fluids* 2008; 45: 371–422.

19. Eroglu H and Chigier N. Wave characteristics of liquid jets from airblast coaxial atomizers. *Atomizat Sprays* 1991; 1: 349–366.

20. Villermaux E, Rehab H and Hopfinger E. Breakup regimes and self-sustained pulsations in coaxial jets. *Meccanica* 1994; 29: 393–401.

21. Villermaux E and Clanet C. Life of a flapping liquid sheet. *J Fluid Mech* 2002; 462: 341–363.

22. Varga CM, Lasheras JC and Hopfinger EJ. Initial breakup of a small-diameter liquid jet by a high-speed gas stream. *J Fluid Mech* 2003; 497: 405–434.

23. Duke D, Honnery D and Soria J. Experimental investigation of nonlinear instabilities in annular liquid sheets. *J Fluid Mech* 2012; 691: 594–604.

24. Marmottant P and Villermaux E. On spray formation. *J Fluid Mech* 2004; 498: 73–111.

25. Vadivukkarasan M and Panchagnula MV. Helical modes in combined Rayleigh–Taylor and Kelvin–Helmholtz instability of a cylindrical interface. *Int J Spray CombustDyn* 2016; 8: 219–234.

26. Matas JP and Cartellier A. Flapping instability of a liquid jet. *Comptes Rendus Mécan* 2013; 341: 35–43.

27. Odier N, Balarac G, Corre C, et al. Numerical study of a flapping liquid sheet sheared by a high-speed stream. *Int J Multiphase Flow* 2015; 77: 196–208.

28. Hardalupas Y and Whitelaw J. Characteristics of sprays produced by coaxial airblast atomizers. *J Propul Power* 1994; 10: 453–460.

29. Charalampous G, Hadjiyiannis C and Hardalupas Y. Comparative measurement of the breakup length of liquid jets in airblast atomisers using optical connectivity, electrical connectivity and shadowgraphy. *Measurement* 2016; 89: 288–299.

30. Heilig A, Kaiser M and Dinkelacker F. Near nozzle high-speed measurements of the intact core for diesel spray. In: *Proceeding of 12th triennial international conference on liquid atomization and spray systems*, Heidelberg, Germany, 2–6 September 2012.

31. Linne M. Imaging in the optically dense regions of a spray: a review of developing techniques. *Prog Energy Combust Sci* 2013; 39: 403–440.

32. Patte-Rouland B, Lalizel G, Moreau J, et al. Flow analysis of an annular jet by particle image velocimetry and proper orthogonal decomposition. *Measure Sci Technol* 2001; 12: 1404.

33. Arienti M and Soteriou MC. Time-resolved proper orthogonal decomposition of liquid jet dynamics. *PhysFluids* 2099; 21: 112104.

34. Charalampous G, Hadjiyiannis C and Hardalupas Y. Proper orthogonal decomposition analysis of photographic and optical connectivity time resolved images of an atomising liquid jet. In: *24th annual conference on liquid atomization and spray systems, Estoril, Portugal*, 5–7 September 2011.

35. Danlos A, Ravelet F, Coutier-Delgosha O, et al. Cavitation regime detection through proper orthogonal decomposition: dynamics analysis of the sheet cavity on a grooved convergent–divergent nozzle. *Int J Heat Fluid Flow* 2014; 47: 9–20.

36. Rajamanickam K and Basu S (2017) On the dynamics of vortex–droplet interactions, dispersion and breakup in a coaxial swirling flow. *J Fluid Mech* 2017; 827: 572–613.

37. Sirovich L. Turbulence and the dynamics of coherent structures. I. Coherent structures. *Quarterl Appl Math* 1987a; 45: 561–571.

38. Sirovich L. Turbulence and the dynamics of coherent structures. II. Symmetries and transformations. *Quarterl Appl Math* 1987b; 45: 573–582.

39. Hardalupas Y, Taylor A and Whitelaw J. Mass flux, mass fraction and concentration of liquid fuel in a swirl-stabilized flame. *Int J Multiphase flow* 1994; 20: 233–259.

40. Matas JP, Hong M and Cartellier A. Stability of a swirled liquid film entrained by a fast gas stream. *PhysFluids* 2014; 26: 042108.

41. Chigier N and Dumouchel C. Atomization of liquid sheets. *Recent Adv Spray Combust* 1996; 1: 241–259.

42. Chigier N and Beer J. The flow region near the nozzle in double concentric jets. *J Basic Eng* 1964; 86: 797–804.